AFRL-SN-RS-TR-1998-22
Final Technical Report
March 1998

PULSE PROPAGATION THROUGH FIBER BRAGG GRATINGS

Rensselaer Polytechnic Institute

Joseph W. Haus

APPROVED FOR PUBLIC RELEASE; DISTRIBUTION UNLIMITED.

AIR FORCE RESEARCH LABORATORY
SENSORS DIRECTORATE
ROME RESEARCH SITE
ROME, NEW YORK

This report has been reviewed by the Air Force Research Laboratory, Information Directorate, Public Affairs Office (IFOIPA) and is releasable to the National Technical Information Service (NTIS). At NTIS it will be releasable to the general public, including foreign nations.

AFRL-SN-RS-TR-1998-22 has been reviewed and is approved for publication.

APPROVED: James P Theimer

JAMES P. THEIMER
Project Engineer

FOR THE DIRECTOR: Robert G. Polce

ROBERT G. POLCE, Acting Chief
Rome Operations Office
Sensors Directorate

If your address has changed or if you wish to be removed from the Air Force Research Laboratory Rome Research Site mailing list, or if the addressee is no longer employed by your organization, please notify AFRL/SNDR, 25 Electronic Parkway, Rome, NY 13441-4514. This will assist us in maintaining a current mailing list.

Do not return copies of this report unless contractual obligations or notices on a specific document require that it be returned.

REPORT DOCUMENTATION PAGE	Form Approved OMB No. 0704-0188

1. AGENCY USE ONLY *(Leave blank)*	2. REPORT DATE	3. REPORT TYPE AND DATES COVERED
	March 1998	Final Feb 96 - Feb 97

4. TITLE AND SUBTITLE

PULSE PROPAGATION THROUGH FIBER BRAGG GRATINGS

5. FUNDING NUMBERS

C - F30602-96-2-0056
PE - 62702F
PR - 4600
TA - P5
WU - PF

6. AUTHOR(S)

Joseph W. Haus

7. PERFORMING ORGANIZATION NAME(S) AND ADDRESS(ES)

Rensselaer Polytechnic Institute
110 Eighth Street
Troy NY 12180-3590

8. PERFORMING ORGANIZATION REPORT NUMBER

N/A

9. SPONSORING/MONITORING AGENCY NAME(S) AND ADDRESS(ES)

Air Force Research Laboratory/SNDR
25 Electronic Parkway
Rome NY 13441-4514

10. SPONSORING/MONITORING AGENCY REPORT NUMBER

AFRL-SN-RS-TR-1998-22

11. SUPPLEMENTARY NOTES

Air Force Research Laboratory Project Engineer: James Theimer/SNDR/(315) 330-4870

12a. DISTRIBUTION AVAILABILITY STATEMENT

Approved for public release; distribution unlimited.

12b. DISTRIBUTION CODE

13. ABSTRACT *(Maximum 200 words)*

A model was constructed to describe pulse propagation and frequency conversion in fiber Bragg gratings. The theoretical issues connected with pulse propagation in fibers with fiber Bragg gratings as dispersive elements were examined. The elements can also be designed for use as linear or nonlinear optoelectronic devices. The project included computational and analytical calculations on the amplitude equations, derived by a multiple-scales technique, and the results were tested against exact numerical computations. The computational effort was performed on Numerical Intensive Computers, mainly RS6000 workstations.

The multiple-scales perturbation theory is used to derive a set of coupled-mode equations valid for electromagnetic wave propagation in a weakly periodic, nonlinear medium with periodicity on the order of a wavelength. This is applied to a problem where the medium has a X(2) response and find that the second-harmonic signal generated is enhanced when the fundamental is tuned near the band edge. Results are given for a possible experiment with optical fibers.

14. SUBJECT TERMS

Fiber Laser, Fiber Bragg Grating, Second Harmonic Generation

15. NUMBER OF PAGES

28

16. PRICE CODE

17. SECURITY CLASSIFICATION OF REPORT	18. SECURITY CLASSIFICATION OF THIS PAGE	19. SECURITY CLASSIFICATION OF ABSTRACT	20. LIMITATION OF ABSTRACT
UNCLASSIFIED	UNCLASSIFIED	UNCLASSIFIED	UL

Abstract

We constructed a model to describe pulse propagation and frequency conversion in fiber Bragg gratings. This research was conducted in cooperation with members of the Photonics Center, where measurements will be made on the pulses. The PI and his group examined the theoretical issues connected with pulse propagation in fibers with fiber Bragg gratings as dispersive elements. The elements can also be designed for use as linear or nonlinear optoelectronic devices. The project included computational and analytical calculations on the amplitude equations, derived by a multiple-scales technique, and the results ere tested against exact numerical computations. The computational effort was performed on the Numerical Intensive Computers, mainly RS6000 workstations, at Rensselaer Polytechnic Institute.

The multiple-scales perturbation theory is used to derive a set of coupled-mode equations valid for electromagnetic wave propagation in a weakly periodic, nonlinear medium with periodicity on the order of a wavelength. We apply this to a problem where the medium has a $\chi^{(2)}$ response and find that the second-harmonic signal generated is enhanced when the fundamental is tuned near the band edge. Results are given for a possible experiment with optical fibers.

The research further developed a working relationship with members of the Photonics Center in Rome, NY with joint publications. For this project to be successful, I kept in close communications with the experimental effort by frequent visits.

Table of Contents

List of Figures

Summary of Accomplishments

Under the grant, the following tasks were accomplished:

1. An analytical description of fiber grating using the multiple scales method was developed. This method allows accurate modeling of fiber Bragg gratings and can be used to examine pulse propagation in the devices.

2. Numerical calculations of Bragg gratings have been made using a numerical transfer matrix method and an analytical Bloch-Floquet function analysis; comparison between the two results reveals that the amplitude equations give numerically identical results over the parameter range of physical interest. The group velocity and effective nonlinear response have been analyzed by this method.

3. Regular trips to the Photonics Center were made during to discuss research progress and learn about problems that could benefit from mutual collaboration. Several items of interest were using a modelocked fiber laser being setup by Walter Kaechele with a cross-correlator to study pulse propagation in the 1.5 μm wavelength regime through fiber Bragg gratings.

4. A multiple scales analysis of fiber Bragg gratings with optical nonlinearities were analyzed. The fiber medium can develop strong second-harmonic radiation and we predict that the conversion efficiency can be improved by an order of magnitude. Realistic calculations to study the phenomenon were made and comparison between the numerical and exact results, when possible, gave excellent agreement. The detailed numerical evaluation of the results show that the concept of resonant enhancement has great promise. A paper on these results was accepted for publication.

5. Travel to the Photonics Laboratory to discuss future experiments and develop further results continued on a regular basis. Trips were made to AFOSR workshop in Tucson, AR on October 9-12, 1996 and to the annual Optical Society of America meeting in Rochester, NY October 20-25, 1996. Results were presented on the research progress and informal discussions with leading scientists generated interest in our work.

6. The PI received a photonic crystal sample from Mark Bloemer, who is at the U.S. Army Missile Command. Walter Kaechele at Photonics Center planned experiments on the sample to examine the group velocity changes at the band edge and related linear and nonlinear properties of the device. We were interested in determining the feasibility of the photonic device for true time delay in RF photonics.

1 Introduction

Wave propagation in periodic dielectric materials is useful for developing a number of photonic devices[1], such as distributed feedback lasers[2] and Bragg grating filters[3]. The transmission is characterized by large dispersion of the pulse and the appearance of stop bands when the Bragg conditions are met. Recently, especially large group velocity delays have been reported at the edge of the stop band, where the transmission is near unity and at the same time, the pulse experiences no appreciable change in its shape[4].

This report is devoted to an analysis of second-harmonic frequency conversion in weakly periodic media with material periodicity chosen to be on the order of the fundamental harmonic wavelength. The results are accepted as a publication in the Physical review A. The tools of our analysis are multiple-scales perturbation theory[5] and we carry out the calculations to demonstrate the potential for using a band edge resonance in Bragg gratings. A separate paper deals with the numerical computations for deep gratings[6], but the qualitative understanding gleaned from the present analysis carries over to the analysis of deep gratings. Phase matching multi-wave interactions by periodic structures was perhaps first discussed some time ago by Armstrong et al.[7] and by Bloembergen and Sievers[8].

Three types of phase matching were proposed by Armstrong et al.[7] for efficient harmonic generation. Among them, it was proposed to periodically replace the nonlinear medium by its inversion image every coherence length, which is proportional to the reciprocal of the phase mismatch wavenumber. This is called quasi-phase matching; the nonlinear susceptibility changes sign, but the linear properties of the medium are the same. Generally, the coherence length is orders of magnitude longer than the fundamental wavelength. Theoretically, quasi-phase matching preceeded birefringent phase matching, but it was not experimentally feasible until recently, when periodic poling of the domains in a ferro-electric crystal was developed[9]. Other concepts similar to phase matching were also proposed[10]. For quasi-phase matching to be efficient, the length scale of the material periodicity is on the order of the coherence length; for this length scale periodically varying the nonlinear coefficient is important.

However, there are some signaling problems where the material periodicity is on the order of a wavelength. Here the linear properties of the medium become important and can be used to reduce the phase mismatch arising from nonlinear wave mixing. In this regime, because of the chosen periodicity, only the spatial D.C. component of the (possibly) periodically varying nonlinear coefficient is required. We dub this band-edge phase matching; it is distinct from other forms of phase matching, such as using a defect mode in the periodic structure[11, 12]. Band edge phase matching is so chosen because the fundamental wavelength is near the band edge of the first stop band in the structure and forward-backward wave coupling is resonant. Band edge phase matching can be considered the converse of quasi-phase matching in terms of which medium properties are homogeneous or periodic. In quasi-phase matching the linear medium appears homogeneous and the nonlinear medium is periodic with the period chosen to be of the order of

the coherence length. However, in band edge phase matching the linear medium is periodic and the nonlinear medium appears homogeneous with the periodicity on the order of a wavelength.

As an application of a second-harmonic medium for the processes discussed in this paper, we propose the use of silica glass fibers. Despite the disorder in glass, second-harmonic generation was observed, first in fibers[13, 14], then in bulk glasses[15], as well. Conversion efficiency approaches several percent.

A fiber Bragg grating is an example of a weakly periodic medium. They have a number of applications; filters, taps and wavelength division multiplexers are a few examples, but others have been demonstrated, such as, laser wavelength control, mode conversion in fibers and distributed Bragg reflectors[3]. Furthermore, chirped fiber Bragg gratings have been used to compress pulses broadened by self–phase modulation. For instance, pulses have been compressed from 2 ps duration to less than 200 fs duration[16].

Nonlinear optical mixing effects in fibers can incorporate Bragg gratings to improve the optical conversion of radiation. The design features require good overlap of the optical energy in the fiber grating; advantages are: a reduced, grating-dependent group velocity to increase the interaction time of the waves in the grating, matching of the phase velocities, and band edge resonance to increase the mode amplitude in the structure. The design of periodic structures will lead to higher conversion efficiency, more compact structures, and lower input power requirements. Enhancement of conversion efficiency in deep gratings has been numerically examined[6], but so far no complete analysis of the problem has been made, nor has the problem been examined in fibers. This paper is intended to place the previous findings on a firm mathematical footing; in this we are partially successful by analyzing the case of weakly periodic gratings with periodicity on the order of a wavelength.

In applying multiple scales to the time-dependent pulse problem, we assume the medium to have chromatic dispersion even at the lowest perturbative order. This is slightly different from the usual Kronig-Penney model, where chromatic dispersion is neglected[1]. Time-dependent secularity conditions are different for chromatic dispersive and non-dispersive problems and must be handled separately. However, for the time-independent CW problem, multiple scales can handle both the chromatic dispersive and non-dispersive cases at once, because secularity conditions reduce to those of spatial harmonic Fourier terms, provided the physical problem can be reduced to a finite set of spatial oscillators. We derive evolution equations for the chromatic dispersion case; and for the continuous wave problem, we derive results with chromatic dispersion and then show how the parameters reduce to the dispersionless case to illustrate what is obtained in Kronig-Penney-type models. Note that for band edge phase matching to occur, chromatic dispersion is required in order to offset the Bragg grating dispersion.

2 Coupled-mode Equations

We consider a wave incident upon a nonlinear medium. The medium has a periodic modulation of the dielectric constant; for the one-dimensional case the form of Maxwell's equation is

$$\frac{\partial^2 E}{\partial z^2} - \frac{1}{c^2}\frac{\partial^2 D_L}{\partial t^2} = \frac{4\pi}{c^2}\frac{\partial^2 P^{NL}}{\partial t^2}. \tag{1}$$

D_L is the linear displacement field, which is related to the electric field by the following constitutive relation

$$D_L(z,t) = \int_{-\infty}^{t} \epsilon(z, t-t')E(z,t')dt'. \tag{2}$$

The function $\epsilon(z,t)$ is the dielectric function; it is periodic in z and the medium is dispersive. P^{NL} is the nonlinear polarization contribution, which for our present case is a second-order nonlinearity:

$$P^{NL} = \lambda\chi^{(2)}E^2. \tag{3}$$

Here λ is a parameter that multiplies a perturbative contribution; there are five small parameters in our analysis and this parameter serves as a bookkeeping device. In this context λ is a dimensionless parameter that will be set to one after the perturbation analysis is carried out; it serves to identify all the contributions of a given perturbative order.

The coefficient $\chi^{(2)}$ governs three-wave mixing processes, e.g. sum- and difference-frequency and second-harmonic generation. The analysis given hereafter can also be applied to a number of three-wave mixing processes, but we restrict our attention to second-harmonic generation. The analysis can also be extended to include four-wave mixing by introducing a third-order susceptibility.

Before deriving the coupled-mode equations, Eq. (2) is rewritten by introducing the Fourier transform relation

$$\epsilon(z,t) = \int \hat{\epsilon}(z,\omega)e^{-i\omega t}d\omega. \tag{4}$$

The function $\hat{\epsilon}(z,\omega)$ is complex and its real and imaginary parts are denoted by the subscripts r and i, resp. By using the Taylor series expansion of $\hat{\epsilon}(z,\omega)$, Eq. (2) can be expressed in a local form

$$D_L(z,t) = \hat{\epsilon}(z, i\frac{\partial}{\partial t})E(z,t). \tag{5}$$

This expression is well suited to the multiple-scales analysis given below. The real part of the dielectric function is of order unity, but the imaginary part is considered to be weak,i.e. $\hat{\epsilon}(\omega) = \hat{\epsilon}_r(\omega) + i\lambda\hat{\epsilon}_i(\omega)$. The function $\hat{\epsilon}$ is a periodic function in z. For a weakly periodic medium we assume the form

$$\hat{\epsilon}(z,\omega) = \hat{\epsilon}(\omega) + \lambda 2\Delta\hat{\epsilon}(\omega)\cos(2\pi z/d). \tag{6}$$

Here d is the period of the dielectric variation and $\Delta\hat{\epsilon}(\omega)$ is the amplitude of the spatially periodic component.

2.1 Multiple-scales Analysis

In the multiple-scales analysis[5] the space and time coordinates are expanded in a power series of a small parameter, that we denote as λ; $t_n = \lambda^n t_0$ and $z_n = \lambda^n z_0$. In the past this method has been applied to $\chi^{(2)}$ materials without periodic changes by two of the authors [17]; the procedure parallels that development. The spatial and temporal derivatives are

$$\begin{aligned} \frac{\partial}{\partial t} &= \frac{\partial}{\partial t_0} + \lambda \frac{\partial}{\partial t_1} + ... \\ \frac{\partial}{\partial z} &= \frac{\partial}{\partial z_0} + \lambda \frac{\partial}{\partial z_1} + ... \end{aligned} \tag{7}$$

Similarly, the electric field is also expanded in powers of the perturbation parameter

$$E = E_0 + \lambda E_1 + ... \tag{8}$$

Orders of the perturbation parameter λ are gathered together. Besides the spatial variations of the dielectric function, the nonlinearity and absorption are also considered to be weak, as noted above by the parameter λ. The expansion of the real part of the dielectric function to first order is

$$\hat{\epsilon}_r(i\frac{\partial}{\partial t}) = \hat{\epsilon}_r(i\frac{\partial}{\partial t_0}) + \lambda \hat{\epsilon}_r'(i\frac{\partial}{\partial t_0}) i\frac{\partial}{\partial t_1}. \tag{9}$$

The prime denotes a derivative with respect to the argument of the function, i.e. frequency. The $O(1)$ term in the expansion is

$$L_0 E_0 = \left(\frac{\partial}{\partial z_0^2} - \frac{1}{c^2} \frac{\partial^2}{\partial t_0^2} \hat{\epsilon}_r(i\frac{\partial}{\partial t_0}) \right) E_0 = 0. \tag{10}$$

The solution, when a plane wave is incident at $z = 0$ with a frequency ω and 2ω is expressed as

$$\begin{aligned} E_0 \;=\; & \frac{A_{f1}(z_1,t_1)}{\sqrt{k_1}} e^{i(k_1 z_0 - \omega t_0)} + \frac{A_{b1}(z_1,t_1)}{\sqrt{k_1}} e^{i(-k_1 z_0 - \omega t_0)} + \\ & \frac{A_{f2}(z_1,t_1)}{\sqrt{k_2/2}} e^{i(k_2 z_0 - 2\omega t_0)} + \frac{A_{b2}(z_1,t_1)}{\sqrt{k_2/2}} e^{i(-k_2 z_0 - 2\omega t_0)} + c.c.. \end{aligned} \tag{11}$$

where the wave numbers (k_1, k_2) are obtained from the chromatic dispersion properties of the medium, so that $k_1^2 = \omega^2 \hat{\epsilon}_r(\omega)/c^2$ and $k_2^2 = (2\omega)^2 \hat{\epsilon}_r(2\omega)/c^2$. In our analysis the phase mismatch is also treated as small, i.e. $\lambda \Delta k = (k_2 - 2k_1)$. Note that $\lambda \Delta k z_0 = \Delta k z_1$. Hence the traditional three-wave process is obtained where quadratic nonlinearities dominate. We avoid large phase mismatch because that would lead to an asymptotic regime beyond three-wave mixing (or cascading) [17]. The field amplitudes depend on the slower parameters (z_1, t_1) and the rapid variations of the field appear as a plane-wave

solution of the wave equation. The amplitudes of the fundamental waves (A_{f1}, A_{b1}) and the second-harmonic waves (A_{f2}, A_{b2}) are treated as order unity functions, which multiply the plane-wave solutions.

To first order in λ the equations of motion are

$$\begin{aligned} L_0 E_1 &= \frac{1}{c^2}\left(\frac{\partial^2}{\partial t_0^2} i\hat{\epsilon}_i (i\frac{\partial}{\partial t_0}) E_0\right) - 2\left(\frac{\partial^2}{\partial z_0 \partial z_1} E_0 - \right. \\ &\left. \frac{1}{c^2}\frac{\partial^2}{\partial t_1 \partial t_0}\hat{\epsilon}_r (i\frac{\partial}{\partial t_0}) E_0\right) + \frac{1}{c^2}\frac{\partial^2}{\partial t_0^2}\hat{\epsilon}'_r (i\frac{\partial}{\partial t_0}) i\frac{\partial E_0}{\partial t_1} \\ &+ \frac{2\cos(2\pi z_0/d)}{c^2}\frac{\partial^2}{\partial t_0^2}\Delta\hat{\epsilon}_r (i\frac{\partial}{\partial t_0}) E_0 + \frac{4\pi\chi^{(2)}}{c^2}\frac{\partial^2}{\partial t_0^2} E_0^2 \end{aligned} \tag{12}$$

The chromatic dispersive secular terms are eliminated from the right hand side of Eq. (12), as shown in Refs. [5, 17]. We also choose the grating periodicity, d, so that it is close to one-half of the fundamental harmonic wavelength. The deviation from this condition is denoted by $2\lambda\delta = \frac{2\pi}{d} - 2k_1$ and from that we observe $2\lambda\delta z_0 = 2\delta z_1$. At the fundamental frequency, forward-backward waves are coupled because of the choice of grating periodicity d. The equations of motion for the fundamental frequency envelope functions are given by

$$\begin{aligned} \frac{\partial A_{f1}}{\partial z_1} + \frac{1}{v_{g1}}\frac{\partial A_{f1}}{\partial t_1} &= -\frac{\pi}{d}\frac{\alpha_1}{2} A_{f1} + i\frac{\pi}{d}\kappa A_{b1} e^{i2\delta z_1} + i\frac{\pi}{d} N A_{f2} A_{f1}^* e^{i\Delta k z_1}; \\ -\frac{\partial A_{b1}}{\partial z_1} + \frac{1}{v_{g1}}\frac{\partial A_{b1}}{\partial t_1} &= -\frac{\pi}{d}\frac{\alpha_1}{2} A_{b1} + i\frac{\pi}{d}\kappa A_{f1} e^{-i2\delta z_1} + i\frac{\pi}{d} N A_{b2} A_{b1}^* e^{-i\Delta k z_1}; \end{aligned} \tag{13}$$

The group velocity at the fundamental frequency is $v_{g1} = d\omega/dk_1$; at this perturbation level, the group velocity on the left hand side is that of the homogeneous medium. The normalized absorption coefficient is $\alpha_1 = \frac{d}{\pi}\frac{\omega_0^2}{k_1 c^2}\hat{\epsilon}_i(\omega_0)$ and the normalized grating strength coefficient is $\kappa = \frac{d}{\pi}\frac{\Delta\hat{\epsilon}\omega_0^2}{2k_1 c^2}$. The scaled nonlinear coefficient is $N = \frac{d}{\pi}\frac{\omega_0^2 4\pi\chi^{(2)}}{k_1 c^2\sqrt{k_2/2}}$.

The second-harmonic equations are given by

$$\begin{aligned} \frac{\partial A_{f2}}{\partial z_1} + \frac{1}{v_{g2}}\frac{\partial A_{f2}}{\partial t_1} &= -\frac{\pi}{d}\frac{\alpha_2}{2} A_{f2} + i\frac{\pi}{d} N A_{f1}^2 e^{-i\Delta k z_1}; \\ -\frac{\partial A_{b2}}{\partial z_1} + \frac{1}{v_{g2}}\frac{\partial A_{b2}}{\partial t_1} &= -\frac{\pi}{d}\frac{\alpha_2}{2} A_{b2} + i\frac{\pi}{d} N A_{b1}^2 e^{i\Delta k z_1}; \end{aligned} \tag{14}$$

where the group velocity at the second-harmonic is $v_{g2} = d(2\omega)/dk_2$, where again this is the group velocity of the homogeneous medium, and the normalized absorption coefficient is $\alpha_2 = \frac{d}{\pi}\frac{4\omega_0^2}{k_2 c^2}\hat{\epsilon}_i(2\omega_0)$. The forward- and backward-waves at the second-harmonic are not coupled in the weak-grating limit, unless a second sinusoidal variation of the dielectric function is added so that $\frac{2\pi l}{d} - 2k_2 \sim O(\lambda)$, where l is an integer.

To simplify the equations we scale the length: $z_1 \rightarrow \frac{\pi}{d} z_1$ and the field amplitudes are scaled to the nonlinear coefficient, so that $a_{f1} = N A_{f1} e^{-i\pi\delta_1 z_1/d}$, $a_{b1} = N A_{b1} e^{i\pi\delta_1 z_1/d}$,

$a_{f2} = NA_{f2}e^{i\pi\delta_2 z_1/d}$, and $a_{b2} = NA_{b2}e^{-i\pi\delta_2 z_1/d}$. Here $\delta_1 = \frac{d}{\pi}\delta$ and $\delta_2 = \frac{d}{\pi}\Delta k - 2\delta_1$. The scaled form of the equations of motion for the fundamental fields are

$$\begin{aligned}
\frac{\partial a_{f1}}{\partial z_1} + \frac{d}{\pi v_{g1}}\frac{\partial a_{f1}}{\partial t_1} &= -\frac{\alpha_1}{2}a_{f1} - i\delta_1 a_{f1} + i\kappa a_{b1} + i a_{f2}a_{f1}^*; \\
-\frac{\partial a_{b1}}{\partial z_1} + \frac{d}{\pi v_{g1}}\frac{\partial a_{b1}}{\partial t_1} &= -\frac{\alpha_1}{2}a_{b1} - i\delta_1 a_{b1} + i\kappa a_{f1} + i a_{b2}a_{b1}^*.
\end{aligned} \tag{15}$$

The scaled equations for the second harmonic become:

$$\begin{aligned}
\frac{\partial a_{f2}}{\partial z_1} + \frac{d}{\pi v_{g2}}\frac{\partial a_{f2}}{\partial t_1} &= -\frac{\alpha_2}{2}a_{f2} + i\delta_2 a_{f2} + i a_{f1}^2; \\
-\frac{\partial a_{b2}}{\partial z_1} + \frac{d}{\pi v_{g2}}\frac{\partial a_{b2}}{\partial t_1} &= -\frac{\alpha_2}{2}a_{b2} + i\delta_2 a_{b2} + i a_{b1}^2.
\end{aligned} \tag{16}$$

The above equations were derived for pulses in strongly chromatic dispersive media. For the CW envelope, it does not matter whether the medium is chromatic or achromatic, because the spatial-dependent equations remain the same. However, for pulses in weakly dispersive or achromatic materials, the evolution equations are quite different and the above equations do not apply. The above equations were derived under the assumption that grating dispersion is used to compensate chromatic dispersion.

2.2 Band-edge Phase Matching

The weak grating differs from the homogeneous medium through the addition of two parameters (δ_1, κ), as shown in Eqs. (15,16). Harmonic enhancement is obtained by careful choices of these parameters, and based on the dispersion properties of the material. Note that in this model chromatic dispersion dominates grating dispersion and the results obtained here are different from the usual Kronig-Penney models[1], that neglect chromatic dispersion.

It must be mentioned, that the parameters (δ_1, δ_2) can be related to the frequency detuning $\omega - \omega_0 = \lambda\Delta$. Here $\omega_0 = \frac{\pi c}{dn(\omega_0)}$, which is the scaled frequency for the center of the first stop band. From the previous definitions of (δ_1, k_1) we find

$$\frac{d}{\pi}k_1(\omega) = 1 - \lambda\delta_1 = \frac{d}{\pi}\frac{\omega}{c}n(\omega) \tag{17}$$

Expanding in a Taylor series about ω_0 we obtain

$$\frac{d}{\pi}k_1(\omega_0) = 1 + \lambda\Delta\left[\frac{1}{\omega_0} + \frac{n'(\omega_0)}{n(\omega_0)}\right]. \tag{18}$$

The prime denotes a derivative with respect to angular frequency. Therefore, the scaled deviation parameter δ_1 becomes:

$$\delta_1 = -\Delta \left[\frac{1}{\omega_0} + \frac{n'(\omega_0)}{n(\omega_0)} \right]. \tag{19}$$

For a material with no chromatic dispersion, i.e. $n(\omega) = constant$, only the first term is relevant in Eq. (19) and

$$\frac{d}{\pi} k_1(\omega_0) = 1 + \frac{\lambda \Delta}{\omega_0}. \tag{20}$$

This is expected in the Kronig-Penney-type models.

From Eq. (19), δ_1 is proportional to the frequency detuning Δ multiplied by a function of ω_0. The parameter δ_2 is the difference between the phase mismatch Δk and $2\delta_1$ and is given as

$$\delta_2 = \frac{d}{\pi} \Delta k - 2\delta_1. \tag{21}$$

The band-edge phase matching is obtained by choosing $\delta_2 = 0$. We choose δ_1 to offset the phase mismatch Δk due to chromatic dispersion. This implies the alternate condition:

$$n(2\omega) - n(\omega) = \frac{\pi c \delta_1}{\omega d}. \tag{22}$$

At ω_0 this is approximately:

$$n(2\omega_0) - n(\omega_0) + \lambda\Delta[2n'(2\omega_0) - n'(\omega_0)] = \frac{\pi c \delta_1}{d(\omega_0 + \lambda\Delta)}. \tag{23}$$

If the dispersion is such that $2n'(2\omega_0) - n'(\omega_0) \sim O(\lambda)$, then it may be neglected. We define $\Omega = \omega_0 + \lambda\Delta$. Under these approximations the band-edge phase matching condition becomes

$$n(2\omega_0) - n(\omega_0) = \frac{\pi c \delta_1}{d\Omega}. \tag{24}$$

There are two cases when the band edge phase matching condition cannot be obtained. These occur when $\Delta k = 0$ or $\delta_1 = 0$, independently. The first case denotes the material is chromatically non-dispersive; from Eqs. (19,21), we see that $\delta_2 = -2\delta_1 = 2\Delta/\omega_0$. Here we have a Kronig-Penney-type model with only a Bragg grating and there is no chromatic dispersion to offset. The second case shows that $\delta_2 = d\Delta k/\pi$. Here the material is chromatic, but the detuning from the band gap center frequency is zero because of Eq. (19). Here the transmission is attenuated and the second-harmonic generation is not efficient.

To get the most out of band-edge phase matching, we have to utilize the two independent grating parameters (δ_1, κ). The best value for δ_1 may be inferred without solving Eqs. (15,16), but adjusting κ requires the examination of solutions. By imposing the condition $\delta_2 = 0$, the chromatic dispersion can be compensated by the dispersion of the Bragg grating, i.e. adjusting δ_1. At the band edge the phases introduced by forward- and backward-wave coupling change the phases of the waves in the material and this

condition no longer assures the best conversion efficiency, as will be illustrated below. κ can be adjusted by changing the modulation depth $\Delta\hat{\epsilon}$, so that the best phase matching is concurrently coincident with a transmission resonance of the grating. The transmission resonances, discussed below, are further evidence of strong forward-backward wave coupling and this leads to a an enhancement of the second-harmonic field.

2.3 Steady-state, Non-depleted Solution

The equations can be solved for the non-depleted pump and steady-state fields. This case illustrates the essential desirable features of the grating that enhance the nonlinear response of the material. Absorption is also neglected.

The steady-state equations for the fundamental field amplitude are

$$\frac{\partial a_{f1}}{\partial z_1} = -i\delta_1 a_{f1} + i\kappa a_{b1} \tag{25}$$

$$\frac{\partial a_{b1}}{\partial z_1} = i\delta_1 a_{b1} - i\kappa a_{f1} \tag{26}$$

Defining $\Delta_1 = \sqrt{\delta_1^2 - \kappa^2}$, which is the effective wavenumber for the envelope on the z_1-scale, one can can obtain the corresponding grating group velocity (for the infinite medium)

$$V_G = \Delta_1/\delta_1. \tag{27}$$

This is not the same as the group velocities appearing on the left hand side of Eqs. (15) and (16), but a correction to the group velocity in second-order perturbation theory. The solutions to the above equations are

$$a_{f1}(z) = \left(\cos(\Delta_1 z_1) - \frac{i\delta_1}{\Delta_1}\sin(\Delta_1 z_1)\right) a_{f1}(0) + \frac{i\kappa}{\Delta_1}\sin(\Delta_1 z_1) a_{b1}(0) \tag{28}$$

$$a_{b1}(z) = \left(cos(\Delta_1 z_1) + \frac{i\delta_1}{\Delta_1}\sin(\Delta_1 z_1)\right) a_{b1}(0) - \frac{i\kappa}{\Delta_1}\sin(\Delta_1 z_1) a_{f1}(0) \tag{29}$$

We consider a medium with N periods; in scaled units the sample length is $L = \pi N$. The input field $a_{f1}(0)$ is normalized to 1, and applying the boundary condition that the backward field vanished at L, gives the reflected field amplitude

$$a_{b1}(0) = \frac{i\kappa \sin(\Delta_1 L)}{\Delta_1 \cos(\Delta_1 L) + i\delta_1 \sin(\Delta_1 L)} \tag{30}$$

The transmittance through the structure is simply $T = |a_{f1}(L)|^2$.

The results are illustrated by considering the following index variation $\Delta\hat{\epsilon} = 5 \times 10^{-4}$, with $\epsilon_1 = 1$ and $\epsilon_2 = 1 + 2\Delta\hat{\epsilon}$. The average dielectric constant is 1.0005. Figure 1 is plots

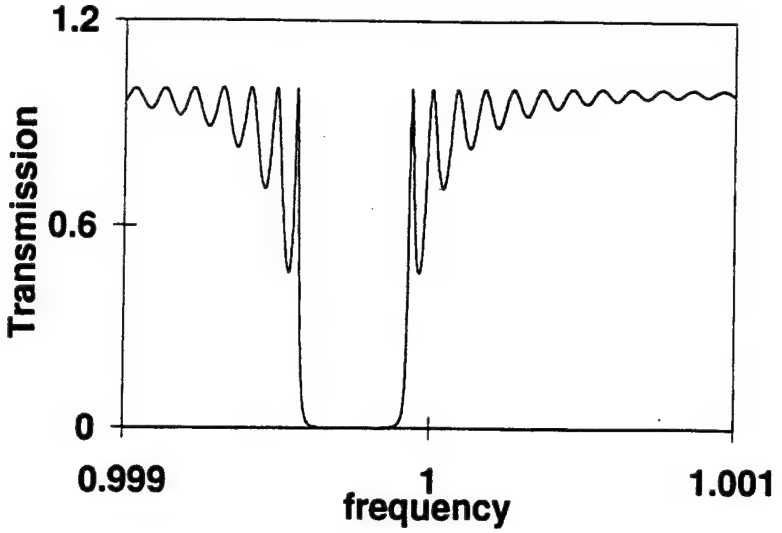

Figure 1: Transmission versus frequency for a 10^4 period grating (or in scaled units $L = \pi 10^4$) with a dielectric variation of $\Delta\hat{\epsilon} = 5 \times 10^{-4}$. The mode-coupled results and the transfer matrix calculations are indistinguishable.

of the transmission $|a_{f1}(L)|^2/|a_{f1}(0)|^2$ versus frequency for $L = \pi 10^4$. The analytically calculated curve is indistinguishable from those generated by a transfer matrix routine with a step index profile whose first Fourier coefficient is identical to $\Delta\hat{\epsilon}$. We note that the center of the gap is displaced from unity because the average refractive index is not unity.

The transmission oscillations at the band edges are called transmission resonances. They have a close correspondence with Fabry-Perot-like resonances of the envelope functions in the structure. The field amplitude corresponding to the first transmission resonance at the lower edge of the stop band is plotted in Figure 2. As would be found for the lowest transmission resonance in a Fabry-Perot etalon, the field amplitude has one maximum. The difference here is that the Fabry-Perot resonance is half a wavelength, while for the Bragg grating, field amplitude is slowly varying over the scale of the wavelength. The input field is normalized to unity. The forward- and backward- propagating amplitudes have a single extremum and their maxima exceeds the input field value. The maximum value increases as the number of periods, N, increases. The maximum field amplitude is proportional to $\Delta\hat{\epsilon}$ and increases with this parameter, as well. For large dielectric contrast between the layers only a few layers suffice to enhance the field beyond its input value[6]. This can be used to design compact frequency conversion structures.

The second-harmonic fields are simply solved by applying the Laplace transform technique to Eq. (16); in general, the solutions are complicated and we do not present them here. In the following sections we will analyze the solutions in detail.

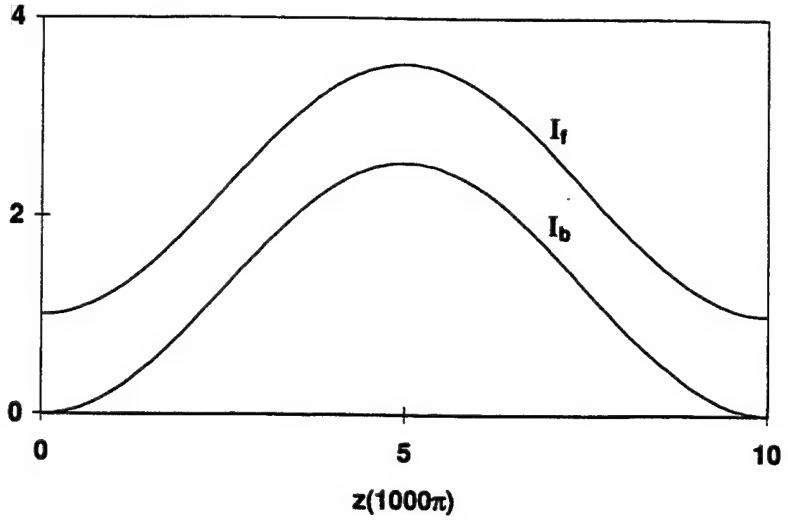

Figure 2: The forward- and backward- propagating field intensities, when the detuning is set at the first transmission maximum on the lower band edge, as a function of position (z in units of $\pi 10^3$). For parameter details see Figure 1.

3 Results

The second-harmonic fields at the transmission maximum are enhanced by the transmission resonance of the fundamental field. In homogeneous media the fields are phase matched, i.e. $\Delta k = 0$, to assure that the best conversion efficiency is achieved. However, as mentioned above, the optimal condition for conversion is not identical to the phase matching condition without the backward-propagating fields, which are coupled by the grating period and lead to the parameter $2\delta_1$ compensating for Δk. The interplay of forward- and backward-fields gives additional position-dependent phase shifts to the complex amplitudes.

Figures 3 and 4 display the behavior of the second-harmonic fields in the medium as a function of frequency, but assuming $\delta_2 = 0$ at each frequency, i.e. Ω is the frequency of the fundamental field. The forward, second-harmonic field is zero at the input, but increases at the output, a maximum increase occurs when the phase matching frequency corresponds to the maximum of the transmission curve, which is also drawn on the side panel.

The output second-harmonic intensity has been scaled to the second-harmonic generated from a perfectly phase matched homogeneous medium of the same length and nonlinear response. The enhancement of the forward- propagating output at the maximum is about 16 times that of the homogeneous case. The second harmonic is roughly proportional to the square of the intensity, so the large second-harmonic can be mainly attributed to the enhanced first harmonic field at the transmission resonance, which is nearly a factor of 4. For a 2.5×10^4 period grating, the enhancement is about 400 times above the homogeneous medium, when the fields are phase matched. Note we remain

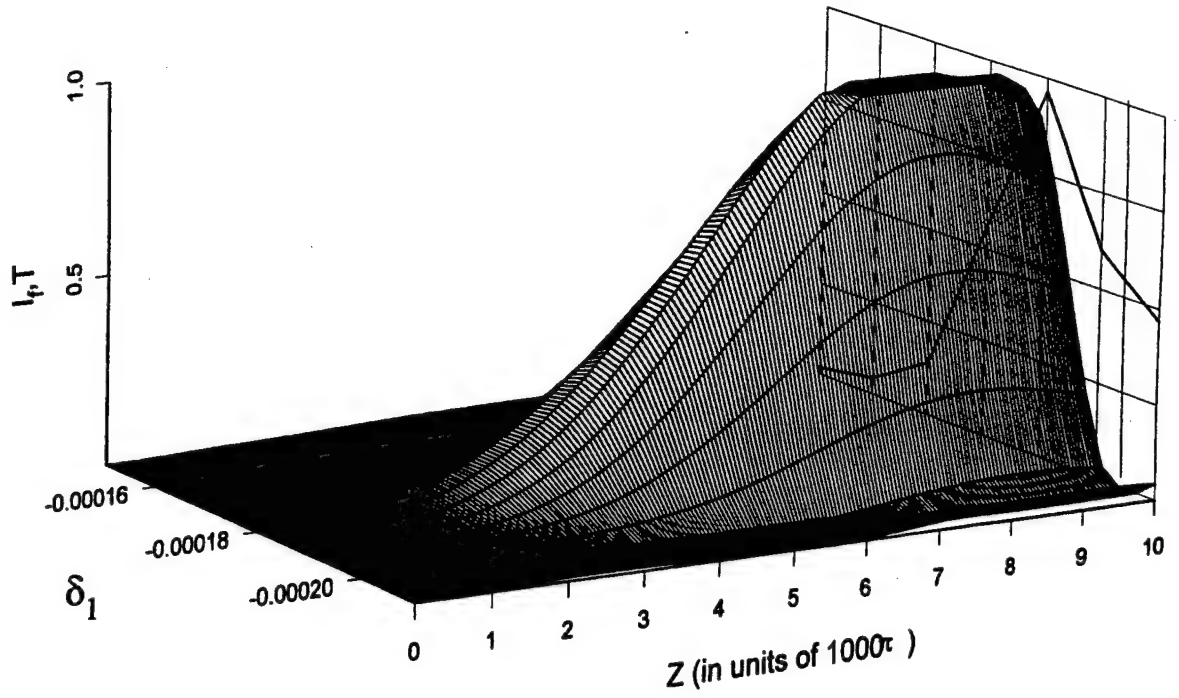

Figure 3: Forward-propagating second-harmonic intensity in the medium versus position and phase matching frequency for a 10^4 period structure. The vertical axis has been scaled by 8. The side panel shows the transmission spectrum for the fundamental wave.

within the non-depleted pump approximation and the second harmonic is still weak compared to the fundamental.

The second-harmonic backward-wave is also enhanced by about a factor of 4 above the homogeneous medium. Again by reference to Figure 1 this is consistent with the enhanced fundamental-harmonic backward-field inside the medium. The forward- and backward-fields form a standing-wave pattern in the sample at the transmission resonance and although the fundamental field is absent in the reflection at the transmission peak, the backward second-harmonic has a maximum there. The backward-propagating second-harmonic intensity is a probe of the backward fundamental field in the medium, just as the forward- propagating second harmonic probes its fundamental field.

Finally, the sharpness of the response with phase matching is gauged from Figure 5 for the forward-propagating second harmonic field. The field has been scaled by a factor of 16 and the side panels display the transmission curves for the fundamental. The maximum for a given value of δ_1 occurs at the first transmission maximum; the output is sharply peaked at that frequency with a spectral width about as wide as the transmission resonance. This occurs for both the forward and the backward (not shown here) fields. The forward-propagating, second-harmonic field is the strongest, since it has the largest field at the transmission resonance, as previously discussed. Since the fields are not phase matched at the upper transmission maximum, there is no perceptible output on this scale of intensities. Also, drawing attention to the side panel on the Ω axis, we

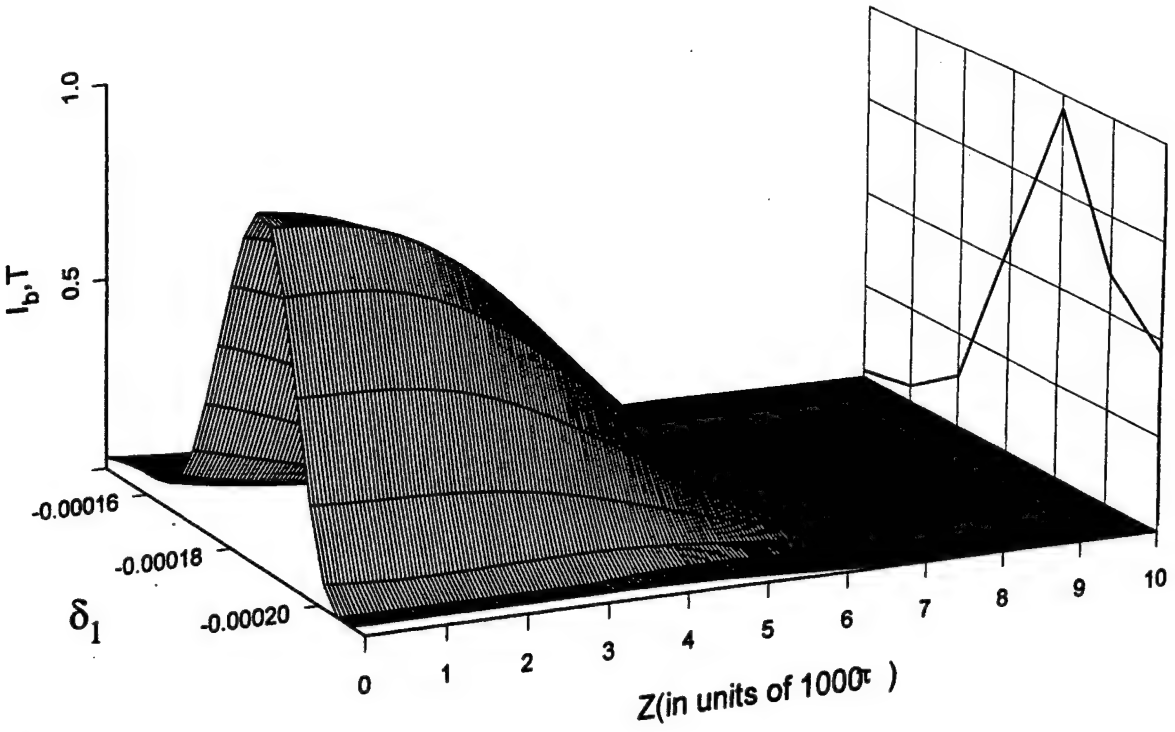

Figure 4: backward-propagating second-harmonic intensity in the medium versus position and phase matching frequency for a 10^4 period structure. The vertical axis has been scaled by 8. The side panel shows the transmission spectrum for the fundamental wave.

note the maximum conversion does not occur when $\delta_2 = 0$ at the first transmission maximum; instead, the best conversion efficiency occurs for $\delta_2 = 0$ at the second transmission maximum. This is a consequence of the additional phase changes due to presence of both forward- and backward-fields in the medium. The weak secondary maxima observed is due to the resonance at the second transmission maximum. Including medium dispersion in the analysis is an important aspect of designing efficient conversion devices.

4 Concluding Remarks

The fields are affected by several factors at the band edge. First, there is a Fabry-Perot type resonance in the field amplitudes, which leads to higher conversion efficiencies inside the structure. The field amplitude is large over a major portion of the volume. Second, the transmission is large, so that all the fundamental field will enter the structure, i.e there is no impedance mismatch. Third, the group velocity at the band edge is small and the fundamental field spends more time inside the structure leading to greater conversion efficiency. Our results are quite distinct from quasi-phase matching, which involves a different length scale; the medium periodicity is chosen on the order of a coherence length and modulating the nonlinear coefficient is important. The contrast with band-edge phase matching is apparent; since the grating periodicity is on the order of a wavelength, the

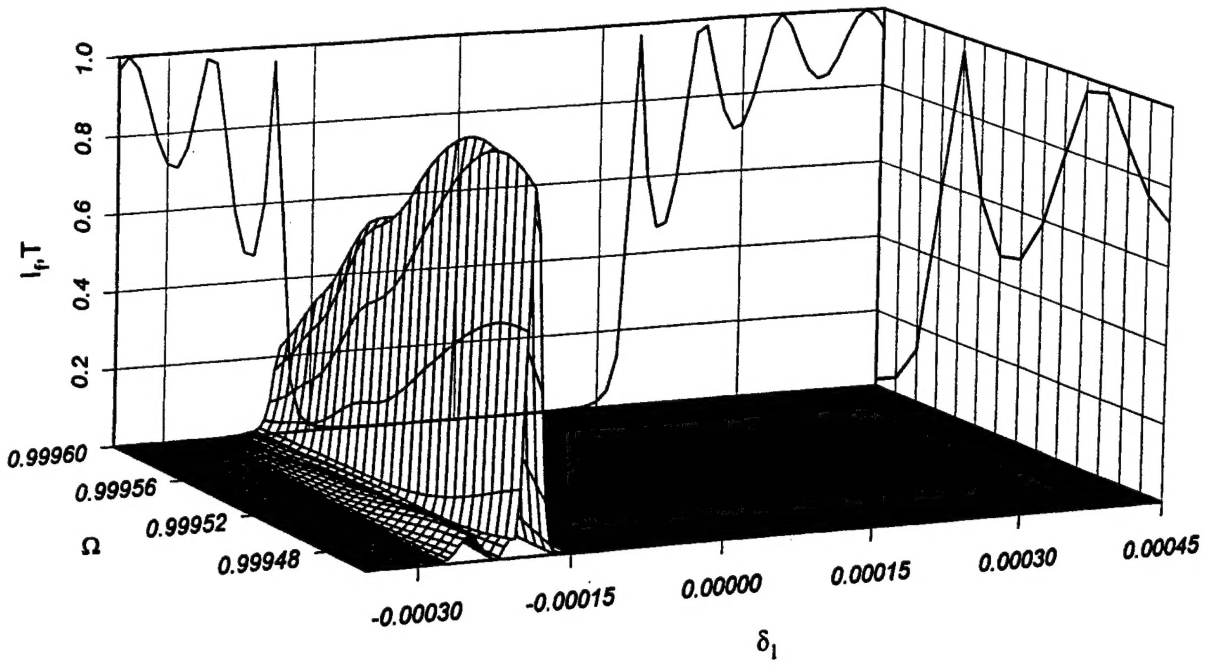

Figure 5: The plot of the forward-propagating second-harmonic intensity in the medium versus phase matching and detuning for a 2.5×10^4 period structure. The vertical axis has been scaled by 16. The side panels show the transmission spectrum for the fundamental wave.

linear properties of the medium are utilized to reduce the phase mismatch, as described by the parameter δ_2.

There are design parameters, whose determination is important for applications of this analysis. The phase matching condition is not easily defined here due to the interaction of the forward- and backward-waves; nevertheless, there are optimal values of δ_1 that provide enhanced conversion. The matching frequency and the transmission maxima should be tuned for the best results. This means that for a given amplitude, $\Delta\hat{\epsilon}$, there is an optimum number of layers that will achieve this condition. The number of layers should be large enough to result in an increased conversion efficiency; on the other hand, the maximum number of layers is set by technological limits, but the larger the number of periods, the sharper the transmission resonances in frequency space (compare Figures 1 and 2). This sets a lower limit on the pulse duration, since if the pulse is too short, then its spectrum extends over several transmission maxima, which leads to pulse dispersion, reflection, and reshaping in the structure.

Second-harmonic fields have been generated in glass hosts, despite the fact that it is on the average centro-symmetric. This centro-symmetry can be broken by adding a static external field or by defects seeded in the medium during the three-wave mixing process. Fiber Bragg gratings written into prepared fibers could be used to demonstrate the resonance enhancement concept. The conversion is already good for the prepared

fiber and it could be further increased by writing a Bragg grating into the fiber. The index change in the core could be of order 0.01 [18] and the overlap of a mode with the core is typically around 75 %, so that the efficiency of the coupling is not significantly reduced[19].

The results presented here apply to a number of nonlinear conversion phenomena. The sum- and difference- frequency generation problems are amenable to the analysis given here. The coupled-mode equations are similar, but now depend linearly on the fundamental field. Third-order processes can also be treated by the same approach; the third-harmonic generation process depends on the cube of the fundamental field and greater efficiency can be achieved by the band edge resonance; there is an additional gap near the third-harmonic frequency, that provides a further resonance condition. For wavelengths below about 400 nm though, absorption will have to be included in the analysis. Other nonlinear processes can also be optimally designed at the band edge, for instance, the stimulated Raman scattering could be suppressed by tuning the fundamental field to the upper, band-edge resonance or the amplification of fields and quantum coherence between the Stokes and anti-Stokes fields[20] could be managed by band-edge changes in the electromagnetic density of states.

There are a number of applications of the concepts useed here. The enhanced second-harmonic (or third-harmonic) signal can be incorporated in a number of time-resolved spectroscopy applications, such as, frequency resolved optical gating (so-called FROG) or recent Zeptojoule measurements to improve the signal-to-noise ratio. It can also be used in a waveguide environment to assist in signal demultiplexing by converting colliding pulses to second-harmonic radiation.

References

[1] A. Yariv and P. Yeh, "Optical Waves in Crystals," (John Wiley and Sons, NY, 1984).

[2] H. Kogelnik and C. V. Shank, J. Appl. Phys. **43**, 2328 (1972); M. Nakamura, A. Yariv, H. W. Yen, S. Somekh, and H. L. Garvin, Appl. Phys. Lett. **22**, 515 (1973).

[3] K. O. Hill, B. Malo, F. Bilodeau and D. C. Johnson, Ann. Rev. Mater. Sci. **23**, 125 (1993).

[4] M. Scalora,R. J. Flynn, S. B. Reinhardt, R. L. Fork, M. J. Bloemer, M. D. Tocci,C. M. Bowden, J. P. Dowling, and R. P. Leavitt, Phys. Rev. E **54**, R1078 (1996).

[5] J. Kevorkian and J. D. Cole, "Perturbation Methods in Applied Mathematics," (Springer Verlag, New York, 1981).

[6] M. Scalora, A. S. Manka, M. J. Bloemer, J. P. Dowling, C. M. Bowden, R. Viswanathan and J. W. Haus, Phys. Rev. A **56**, 3156 (1997).

[7] J. A. Armstrong, N. Bloembergen, J. Ducuing and P. S. Pershan, Phys. Rev. **127**, 1918 (1962).

[8] N. Bloembergen and A. J. Sievers, Appl. Phys. Lett. **17**, 483 (1970).

[9] M. Yamada, N. Nada, M. Saitoh and K. Watanabe, Appl. Phys. Lett. **62**, 435 (1993); W. K. Burns, W. McElhanon and L. Goldberg, IEEE Photon. Tech. Lett. **6**, 252 (1994); M. M. Fejer, G. A. Magerl, D. H. Jundt and R. L. Byers, IEEE J. Quantum Electron. **28**, 2631 (1992); Q. Chen and W. P. Risk, Electron. Lett. **30**, 1516 (1994).

[10] S. Somekh and A. Yariv, Appl. Phys. Lett. **21**, 140 (1972); Opt. Commun. **6**, 301 (1972).

[11] J. Martorell and R. Corbalan, Opt. Commun. **108**, 319 (1994).

[12] J. Trull, R. Vilaseca, J. Martorell and R. Corbalan, Opt. Lett. **20**, 1746 (1995).

[13] Y. Sasaki and Y. Ohmori, Appl. Phys. Lett. **39**, 466 (1981).

[14] U. Osterberg and W. Margulis, Opt. Lett. **11**, 516 (1986).

[15] T. J. Driscoll and N. M. Lawandy, Opt. Lett. **19**, 7 (1994).

[16] J. A. R. Williams, I. Bennion and L. Zhang, IEEE Photon. Tech. Lett. **7**, 491 (1995).

[17] A.G. Kalocsai and J. W. Haus, Phys. Rev. E **52**, 3166 (1995); Phys. Rev. A **49**, 574 (1994).

[18] P. Lamaire, R. M. Atkins, V. Mizrahi and W. A. Reed, Electron. Lett. **29**, 1191 (1993).

[19] G. P. Agrawal, "Fiber-optic Communication Systems", (John Wiley and Sons, NY, 1992) p. 37-39.

[20] K. C. Yeong, J. W. Haus and A. Chizhov, Phys. Rev. A **53**, 3606 (1996).